Chemical Science

ROYAL SOCIETY OF CHEMISTRY

EDGE ARTICLE

View Article Online
View Journal | View Issue

Open Access Article. Published on 15 April 2021. Downloaded on 11/22/2025 9:41:00 PM.
This article is licensed under a Creative Commons Attribution-NonCommercial 3.0 Unported Licence.

Check for updates

Cite this: *Chem. Sci.*, 2021, **12**, 6983

All publication charges for this article have been paid for by the Royal Society of Chemistry

Design of pure heterodinuclear lanthanoid cryptate complexes†

Christian D. Buch,[a] Steen H. Hansen,[a] Dmitri Mitcov,[a] Camilla M. Tram,[a] Gary S. Nichol,[b] Euan K. Brechin[b] and Stergios Piligkos *[a]

Received 18th February 2021
Accepted 14th April 2021

DOI: 10.1039/d1sc00987g

rsc.li/chemical-science

Heterolanthanide complexes are difficult to synthesize owing to the similar chemistry of the lanthanide ions. Consequently, very few purely heterolanthanide complexes have been synthesized. This is despite the fact that such complexes hold interesting optical and magnetic properties. To fine-tune these properties, it is important that one can choose complexes with any given combination of lanthanides. Herein we report a synthetic procedure which yields pure heterodinuclear lanthanide cryptates LnLn*LX_3 (X = NO_3^- or OTf^-) based on the cryptand H_3L = N[$(CH_2)_2$N=CH–R–CH=N–$(CH_2)_2]_3$N (R = *m*-C_6H_2OH-2-Me-5). In the synthesis the choice of counter ion and solvent proves crucial in controlling the Ln–Ln* composition. Choosing the optimal solvent and counter ion afford pure heterodinuclear complexes with any given combination of Gd(III)–Lu(III) including Y(III). To demonstrate the versatility of the synthesis all dinuclear combinations of Y(III), Gd(III), Yb(III) and Lu(III) were synthesized resulting in 10 novel complexes of the form LnLn*$L(OTf)_3$ with LnLn* = YbGd **1**, YbY **2**, YbLu **3**, YbYb **4**, LuGd **5**, LuY **6**, LuLu **7**, YGd **8**, YY **9** and GdGd **10**. Through the use of ^{1}H, ^{13}C NMR and mass spectrometry the heterodinuclear nature of YbGd, YbY, YbLu, LuGd, LuY and YGd was confirmed. Crystal structures of LnLn*$L(NO_3)_3$ reveal short Ln–Ln distances of ~3.5 Å. Using SQUID magnetometry the exchange coupling between the lanthanide ions was found to be anti-ferromagnetic for GdGd and YbYb while ferromagnetic for YbGd.

Introduction

Lanthanide (Ln) molecular materials have attracted strong interest and have been intensively studied in a wide range of areas such as catalysis,[1–5] bioinorganic chemistry,[6,7] Magnetic Resonance Imaging,[8–10] luminescent materials,[11–14] multimodal imaging probes,[15–17] Single-Molecule Magnets (SMMs)[18–21] and Quantum Information Processing (QIP).[22–34] Many of the interesting properties of Ln complexes originate from their special electronic structure, where the 4f subshell is shielded from the environment by the 5s and 5p orbitals.[35] For example, this results in a large unquenched orbital-angular momentum which has been essential to build SMMs[36–38] with record blocking temperatures,[39–41] and leads to sharp absorption and emission bands, due to the lower influence of vibrations on the f–f transitions.

With respect to QIP, Ln complexes form a very exciting but rather unexplored class of molecular materials.[27,42–45] We have recently demonstrated that Yb(trensal),[46] a member of the Ln(trensal) series,[47–54] is a very promising candidate for the realisation of a molecule-based electronic quantum-bit (qubit).[45] Yb(trensal) is one of the few known Ln-based molecular qubits to date. Furthermore, the potential multilevel nature of Ln molecular materials, resulting from the hyperfine interaction of electronic and nuclear angular momenta or from week ligand field splittings of the Stark sublevels in cases where the orbital angular momentum is quenched, can be exploited as an additional resource for the development of quantum logic algorithms.[55–59] In recent ground-breaking work, Grover's quantum algorithm, relevant to identifying an element within an unsorted database, was implemented on the basis of the four nuclear spin wavefunctions of a bis(phthalocyanine) Tb(III) molecular magnet.[60] Nuclear spins were also proposed as physical supports for the implementation of qubits,[28,60] since the contraction of nuclear wave functions shields them from the environment, minimizing decoherence effects. This results in nuclear spins having much longer coherence times than their electronic counterparts. However, this isolation also leads to long manipulation times,[61] which can be circumvented *via* the use of molecular systems in which hyperfine interactions are significant, resulting in faster manipulation time-scales.[62] We very recently demonstrated that Yb(trensal)[46] is a prototypical

[a]*Department of Chemistry, University of Copenhagen, Universitetsparken 5, DK-2100, Copenhagen, Denmark. E-mail: piligkos@chem.ku.dk*

[b]*EaStCHEM School of Chemistry, University of Edinburgh, Edinburgh, UK*

† Electronic supplementary information (ESI) available: Experimental details and characterisation and magnetisation data of **1–10**. Crystallographic data (including structure factors) for $\mathbf{1_N}$–$\mathbf{10_N}$. CCDC 2059654 ($\mathbf{10_N}$), 2059655 ($\mathbf{5_N}$), 2059656 ($\mathbf{7_N}$), 2059657 ($\mathbf{3_N}$), 2059658 ($\mathbf{6_N}$), 2059659 ($\mathbf{1_N}$), 2059660 ($\mathbf{4_N}$), 2059661 ($\mathbf{2_N}$), 2059662 ($\mathbf{8_N}$), 2059663 ($\mathbf{9_N}$). For ESI and crystallographic data in CIF or other electronic format see DOI: 10.1039/d1sc00987g

© 2021 The Author(s). Published by the Royal Society of Chemistry

Open Access Article. Published on 15 April 2021. Downloaded on 11/22/2025 9:41:00 PM.
This article is licensed under a Creative Commons Attribution-NonCommercial 3.0 Unported Licence.

coupled electronic qubit–nuclear qudit[63] (where a qudit is a quantum system comprising more than two levels). The nuclear qudit of the ^{173}Yb isotope nucleus (nuclear spin $I = 5/2$) displayed coherence times of the order of 10 to 10^2 microseconds, similar to the best performing, state-of-the-art, nuclear-spin-based qudits.[64] Most importantly, the electronuclear multilevel structure of the qudit allowed intrinsic implementation of quantum error corrections concerning encoding of both amplitude and phase shift error corrections.[63] QIP algorithms can be performed as a sequence of single qubit rotations and gate operations performed on two entangled qubits. Thus, nuclear spins hosted in molecular magnetic materials are excellent candidates for the implementation of single qubit gates. However, their lack of interaction with the environment creates difficulties for the realization of coupled qubit gates. Hyperfine interactions mix the nuclear and electronic angular momentum wave-functions. Thus, construction of nuclear spin quantum gates appears feasible by simultaneously exploiting the long range coupling of electronic spins *via* magnetic exchange interactions and the hyperfine interaction-induced mixing of the electronic and nuclear angular momenta, at the single-ion level.[65] In order to be individually addressable, the two angular momenta located on the two lanthanide centres composing the quantum gate have to be different. Thus, the need for the controlled synthesis of pure heterometallic complexes arises.

Synthesis of heterometallic Ln complexes is difficult since the 4f elements all have very similar chemistries. This is further compounded by the bonding interaction with ligands being largely ionic in character,[35] resulting in many synthetic protocols producing impurities from homonuclear complexes (*i.e.* scrambling).[66–69] Thus, examples of pure heterometallic Ln complexes remain rare. These are almost solely limited to phthalocyanine[70–73] and DOTA complexes.[74–76] An elegant strategy relying on size selection of dissymmetric ligands has been employed to synthesise heteronuclear Ln complexes without scrambling.[31,33] However, this is only efficient when the included Ln(III) ions are of very different size, greatly limiting the choice of possible combinations.[67]

We present herein a synthetic strategy for the realization of pure heterodinuclear Ln complexes of composition not limited by size selectivity. Thus, for the second half of the lanthanide series (from Gd to Lu, and including Y), our synthetic strategy results in heterodinuclear complexes of arbitrary composition. To illustrate this point, we present the synthesis and characterisation of heterodinuclear complexes LnLn*L containing two large Ln centres (Y, Gd), two small Ln centres (Yb, Lu) and one small (Yb or Lu) and one large (Y or Gd) centre, corresponding to the following 10 complexes: YbGd **1**, YbY **2**, YbLu **3**, YbYb **4**, LuGd **5**, LuY **6**, LuLu **7**, YGd **8**, YY **9** and GdGd **10**. We also demonstrate the solid-state and solution-state stability of **1–10**, and present the static magnetic properties of the paramagnetic members of the family, namely, **1**, **2**, **3**, **4**, **5**, **8** and **10**.

Results and discussion

Synthetic strategy

We initiated a research program to construct pure heterodinuclear Ln complexes the composition of which is not limited by size considerations, meaning that we should also be able to synthesize pure heterodinuclear complexes containing Ln centres of similar size. Given the relevance of Yb(trensal) to QIP,

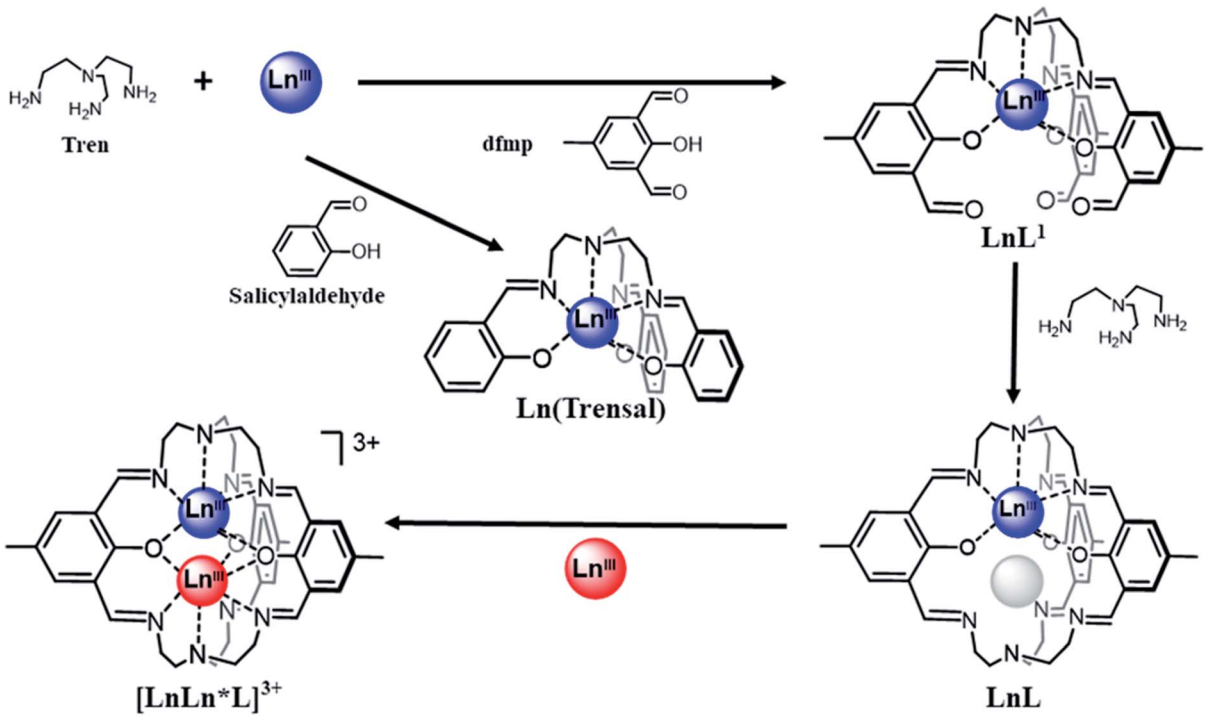

Scheme 1 Strategy for the synthesis of pure heterodinuclear LnLn*L complexes based on the Ln(trensal) motif.

 © 2021 The Author(s). Published by the Royal Society of Chemistry

Open Access Article. Published on 15 April 2021. Downloaded on 11/22/2025 9:41:00 PM.
This article is licensed under a Creative Commons Attribution-NonCommercial 3.0 Unported Licence.

we decided to use the Ln(trensal) motif as the elementary platform upon which our new heterodinuclear complexes would be constructed.

As can be seen from Scheme 1, the heptacoordinated Ln ion in Ln(trensal) occupies all the available coordination positions within the complex. There are therefore no uncoordinated functional sites left to be used as expansion points of the structural motif to accommodate coordination of a second Ln* centre. Thus, use of a ligand bearing additional chemical functions is necessary. In the first instance we used tris(2-aminoethyl)amine (tren) and 2,6-diformyl-*p*-cresol (dfmp), a functionalised derivative of salicylaldehyde. Use of dfmp allows for the synthesis of complexes of type LnL^1 (Scheme 1) that can be regarded as functionalized derivatives of Ln(trensal). Subsequently, the template effect of the Ln centre in LnL^1 was exploited for the condensation of a second tren to create the cryptate complexes LnL, which possess a preformed vacant coordination site that ultimately acts as host for the second Ln centre. In the final step, the second Ln* centre is inserted in the cryptate resulting in the targeted heterodinuclear complexes $[LnLn^*L]X_3$, with X a monoanion. Cryptand complexes are known to be thermodynamically and kinetically stable,[77] with Ln(III) cryptates being considered suitable candidates for MRI contrast agents.[78] Such stability is a prerequisite for surface deposition protocols and, ultimately, inclusion in spintronic devices. To the best of our knowledge only homodinuclear Ln(III) cryptates exist.[78–82]

We have previously presented the synthesis, magnetic and spectroscopic properties of LnL^1 and LnL.[83,84] Both these families of complexes have merits on their own and should not simply be regarded as mere intermediate compounds in the synthesis of our targeted heterodinuclear complexes. LnL^1 contains pendant, reactive carbonyl functions that can be used as anchoring points for surface deposition protocols. These same functionalities can also be exploited in post-synthetic reaction schemes making them truly versatile modules for deposition on various surfaces.[84] LnL have previously been considered as targets for the development of novel MRI contrast agents.[83]

Synthesis and characterisation

Complexes **1–10** were synthesized in a step-wise procedure. First the cryptate LnL was synthesised according to the procedure we have very recently published.[83] To this was then added 3 to 5 equivalents of $Ln^*(OTf)_3 \cdot xH_2O$, depending on the size of the Ln*(III) ion. The resulting yellow pyridine solution was refluxed. Following a workup procedure detailed in the Experimental section, the complexes were isolated as pale yellow powders. Interestingly, **3**, **4** and **7** involving insertion of the smallest Ln(III) ions require the longest refluxing times and the largest surplus of $Ln^*(OTf)_3 \cdot xH_2O$. This indicates that the size of the Ln ion is important for insertion into LnL and that the smallest Ln(III) ions are the most difficult to insert. It should be noted that **10** was synthesized in a slightly different manner to **1–9**, since $GdL \cdot 4H_2O$ could not be isolated.[83] Thus for the synthesis of **10**, *in situ* formation of GdL was followed by addition of Ln*,

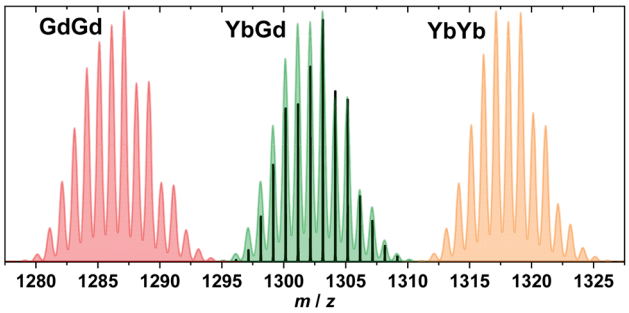

Fig. 1 MALDI positive mode mass spectrum of **1**. Colour code: signal (black), predicted isotope patterns for $[Gd_2L(OTf)_2]^+$ (red), $[YbGdL(OTf)_2]^+$ (green), and $[Yb_2L(OTf)_2]^+$ (orange).

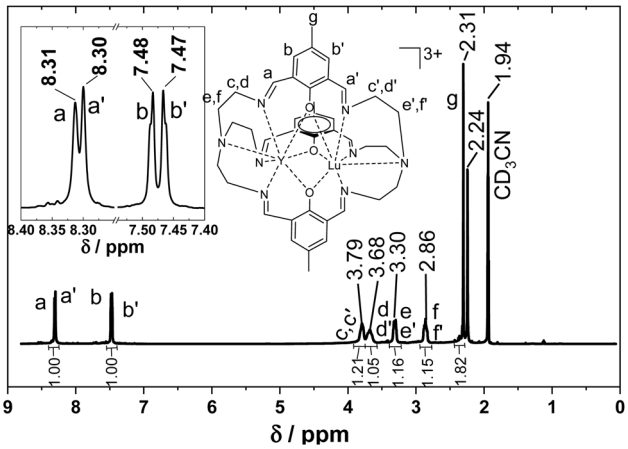

Fig. 2 ^1H NMR of **6** in CD_3CN. The insert shows an enlargement of the four signals between 8.5 and 7.0 ppm.

as described in detail in the Experimental section. The presence of the desired heterodinuclear complexes was confirmed by mass spectrometry (Fig. 1 and S1–S10†). The MALDI mass spectra of **1–10**, reveal no signals stemming from the homodinuclear complexes. Furthermore, the experimental and calculated isotope distribution patterns of the MALDI spectra are in excellent agreement, further confirming the presence of the desired heterodinuclear complexes. ^1H and ^{13}C NMR studies of the diamagnetic complexes ((**6**), (**7**) and (**9**)) also reveal that only the desired heterodinuclear complexes are formed (Fig. 2 and S50–S54†). For (**6**), the ^1H and ^{13}C NMR spectra display signals originating from protons and carbons lying in either the Lu(III) or Y(III) part of the complex with different chemical shifts (Fig. 2 and S50†), but which integrate to the same value. Additionally, IR spectroscopy confirms that both coordination sites in **1–10** are fully occupied as there is a single imine stretch (Fig. S28–S37†).

X-ray crystallography

The precipitates obtained for **1–10** are amorphous. In order to ensure phase purity of the synthesized heterodinuclear complexes, samples were recrystallized from ethanol in the presence of a surplus of Bu_4NNO_3 affording the nitrate

Open Access Article. Published on 15 April 2021. Downloaded on 11/22/2025 9:41:00 PM.
This article is licensed under a Creative Commons Attribution-NonCommercial 3.0 Unported Licence.

analogues LnLn*L$(NO_3)_3$ ($\mathbf{1_N}$–$\mathbf{10_N}$) as microcrystalline precipitates. Single crystals of $\mathbf{1_N}$–$\mathbf{10_N}$ were obtained through slow diffusion of **1–10** with 5 equivalents of Bu_4NNO_3 in ethanol. The complexes (Fig. 3) all crystalise in the tetragonal crystal system, in one of the two enantiomorphic space groups $P4_12_12$ and $P4_32_12$. This is because the helicity of the cryptand ligand around the Ln ions leads to chirality, defining a right (Δ) or left (Λ) helix at each Ln centre, resulting in ΔΔ or ΛΛ chiral complexes (Fig. 4) crystalising in homochiral single crystals. Thus, upon crystallisation the chiral complexes resolve, with the complexes containing the ΔΔ conformation crystallizing in the space group $P4_12_12$ while the ΛΛ conformation is present in the space group $P4_32_12$ (Fig. 4), with the Flack parameter practically equal to zero for both the ΔΔ and ΛΛ enantiomers (Tables S4 and S5†). These two space groups are part of the 65 Sohncke space groups that contain only symmetry operations of the first kind (rotations and translations) and can accommodate chiral molecules.[85] For both space groups the whole complex is contained in the asymmetric unit with eight complexes being in the unit cell. All complexes have similar structures with the two Ln ions being placed inside the cryptand ligand, disordered over the two metal sites (Fig. 3). The Ln ions are hepta-coordinated (LnN_4O_3) by the cryptand ligand, being bonded to three phenoxides, three imines and one tertiary amine. The three phenoxide O-atoms bridge between the two Ln ions. This results in short Ln–Ln distances, measuring between 3.4396(7)–3.5035(7) Å, with $\mathbf{7_N}$ and $\mathbf{10_N}$ having the shortest and longest distance (Table S6†), respectively. Going from $\mathbf{10_N}$ through $\mathbf{8_N}$ and $\mathbf{1_N}$ to $\mathbf{5_N}$ the Ln–Ln distance decreases according to the Ln* in the GdLn* combination being smaller (Table S6†). The Ln ions are also coordinated by one nitrate ion each. The nitrates coordinate to the Ln ions with a short and a long Ln–O bond distance

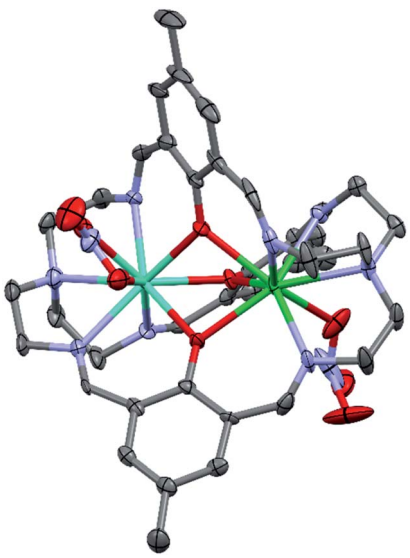

Fig. 3 Crystal structure of the cation of $\mathbf{1_N}$, showing the coordination mode with one bidentate and one monodentate nitrate. Color scheme: C, gray; N, blue; O, red; Gd, cyan; Yb, green. Thermal ellipsoids are set to 50% probability. Hydrogen atoms, counter ions and lattice solvent have been omitted for clarity.

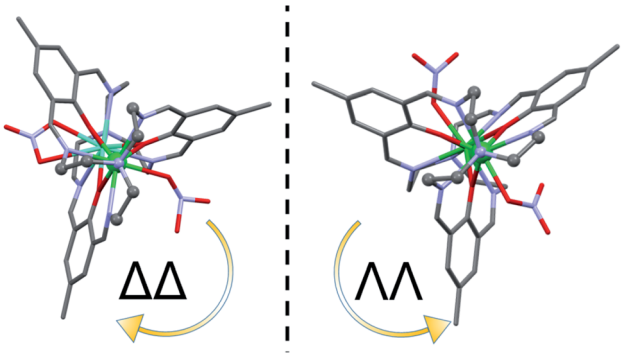

Fig. 4 ΔΔ and ΛΛ enantiomers of the cations of $\mathbf{1_N}$ and $\mathbf{3_N}$, respectively. The complexes are viewed along the pseudo-trigonal axis.

(Table S7†). For $\mathbf{8_N}$–$\mathbf{10_N}$ containing the larger Ln ions (Y and Gd), the two Ln–O bond distances between the nitrate and the Ln ions are differing by 0.2–0.4 Å, suggesting that the nitrate ion is a bidentate ligand towards Ln. For $\mathbf{3_N}$, $\mathbf{4_N}$ and $\mathbf{7_N}$ containing the small Ln ions (Yb and Lu) one of the Ln–O distances shortens a bit while the other one elongates resulting in the two Ln–O bond distances between the nitrate and the Ln ions differing by 0.6–0.9 Å. Thus, the nitrate ions become monodentate ligands. For $\mathbf{1_N}$, $\mathbf{2_N}$, $\mathbf{5_N}$ and $\mathbf{6_N}$ containing both a large (Gd or Y) and a small (Yb or Lu) Ln ion, the difference between the two Ln–O bonds from one nitrate ion becomes 0.4–0.6 Å. Additionally, in $\mathbf{1_N}$–$\mathbf{9_N}$ one of the nitrate ions is disordered over two positions. In this second position the nitrate ion is clearly monodentate as one of the Ln–O distances has been elongated by more than 1 Å (Table S7†). The coordination of the nitrate ion distorts the cryptand ligand such that no threefold symmetry is found around the Ln ion.

PXRD measurements confirm that the isolated powders are isostructural, and have the same structure as the single crystal X-ray structure (Fig. S63 and S64†). PXRD also confirms that the complexes are obtained phase pure. Mass spectrometry reveals $\mathbf{1_N}$–$\mathbf{10_N}$ remain pure heterodinuclear complexes and that no exchange of Ln ions occurs (Fig. S11–S20†). This is also confirmed by NMR spectroscopy where $\mathbf{6_N}$ shows the same splitting in the ^{1}H NMR as **6** (Fig. S60†). Additionally, the NMR spectra of $\mathbf{6_N}$, $\mathbf{7_N}$ and $\mathbf{9_N}$ confirm that the complexes remain dinuclear after the recrystallization (Fig. S60–S62†).

Stability

Based on the discussion of the synthetic protocol, the question as to why $\mathbf{1_N}$–$\mathbf{10_N}$ were not synthesized directly from LnL and Ln*$(NO_3)_3 \cdot xH_2O$, arises. While $\mathbf{1_N}$–$\mathbf{10_N}$ can be synthesized following this route, it also leads to scrambling. This is evident by comparing the mass spectra corresponding to the two synthetic strategies (Fig. S21 and S22†). It is perhaps surprising that such a small change has such a tremendous impact on the control of the LnLn* composition. This indicates that the Lewis basicity of the counterion is crucial. Moreover, we also observed that the choice of solvent has a large impact on the LnLn* composition. For example, exchanging pyridine for PrCN (which has a similar boiling point 115 °C *vs.* 117 °C) leads to

 © 2021 The Author(s). Published by the Royal Society of Chemistry

Open Access Article. Published on 15 April 2021. Downloaded on 11/22/2025 9:41:00 PM.
This article is licensed under a Creative Commons Attribution-NonCommercial 3.0 Unported Licence.

scrambling even when employing $Ln(OTf)_3 \cdot xH_2O$ (Fig. S21 and S23†). This suggests that the basicity of pyridine inhibits the scrambling. The role of pyridine as a base was confirmed by the ^{1}H NMR spectrum of **9** before treatment with THF, where signals from pyridinium triflate are visible (Fig. S59†).

To have a truly versatile heterodinuclear Ln complex, the molecule needs to be as robust as possible. This is especially true if the complex is to be included in spintronic devices where surface deposition techniques require stable components. The cryptate complexes presented herein are all stable in solution for several days. This was confirmed using NMR, where the ^{1}H NMR of **6** dissolved in CD_3CN did not change after seven days (Fig. 2 and S55†). Similar stability was found when dissolved in CD_3OD (Fig. S57 and S58†). To further test the robustness of the complexes 100 equivalents of a third Ln(III) ion were added to a MeOH solution of the complexes. The complexes retain their original LnLn* composition. This was studied by dissolving **4** and **10** in methanol and subjecting them to 100 equivalents of either $Y(OTf)_3 \cdot xH_2O$ or $Lu(OTf)_3 \cdot xH_2O$, respectively. After one week no signals from new species involving either Lu(III) or Y(III) could be observed by mass spectrometry (Fig. S24 and S25†), confirming the robustness of these complexes.

Magnetic properties

The static (d.c.) magnetic properties of $\mathbf{1_N}$–$\mathbf{5_N}$, $\mathbf{8_N}$ and $\mathbf{10_N}$ were investigated by magnetic susceptibility and variable-temperature-variable-field (VTVB) measurements (Fig. 5 and S65–S80†). The susceptibility measurements were performed in a magnetic field, B, of 1000 Oe in the temperature, T, range 2 to 270 K. VTVB measurements were performed in the temperature range 2 to 10 K in applied magnetic fields up to 5 T.

The d.c. susceptibility data of $\mathbf{1_N}$–$\mathbf{5_N}$, $\mathbf{8_N}$ and $\mathbf{10_N}$, are plotted in Fig. 5 as χT products, where $\chi = M/B$ with χ the molar magnetic susceptibility and M the magnetization. At 270 K, the χT products of all measured complexes approach their Curie constants (10.44, 2.57, 2.57, 5.14, 7.87, 7.87 and 15.74 cm^3 K mol^{-1}) with values of 9.91, 2.06, 1.99, 4.30, 7.58, 7.89 and 15.74 cm^3 K mol^{-1}, for $\mathbf{1_N}$, $\mathbf{2_N}$, $\mathbf{3_N}$, $\mathbf{4_N}$, $\mathbf{5_N}$, $\mathbf{8_N}$ and $\mathbf{10_N}$, respectively. Upon decreasing the temperature, the χT product decreases for $\mathbf{2_N}$–$\mathbf{5_N}$, $\mathbf{8_N}$ and $\mathbf{10_N}$ reaching its lowest value at 2 K measuring 1.25, 1.22, 2.39, 7.72, 7.93 and 5.06 cm^3 K mol^{-1}, respectively. This decrease is due to thermal depopulation of excited m_J states in complexes containing one paramagnetic centre ($\mathbf{2_N}$, $\mathbf{3_N}$, $\mathbf{5_N}$ and $\mathbf{8_N}$). For $\mathbf{4_N}$ and $\mathbf{10_N}$ that both contain two paramagnetic centres, the decrease can be attributed to a combination of effects arising from thermal depopulation of excited m_J states and anti-ferromagnetic interactions between the coupled Ln centres. For $\mathbf{4_N}$, thermal depopulation of excited m_J states will prevail at higher temperatures, and the weak exchange interactions will occur at lower temperatures. For $\mathbf{10_N}$, given the magnetically isotropic nature of Gd(III), this picture is inversed. The χT product of $\mathbf{1_N}$ also decreases upon lowering the temperature down to 12 K. Below this temperature the χT product of $\mathbf{1_N}$ rapidly increases, reaching a maximum of 9.44 cm^3 K mol^{-1} at 2 K. This behavior indicates ferromagnetic coupling between the Yb(III) and Gd(III) centres.

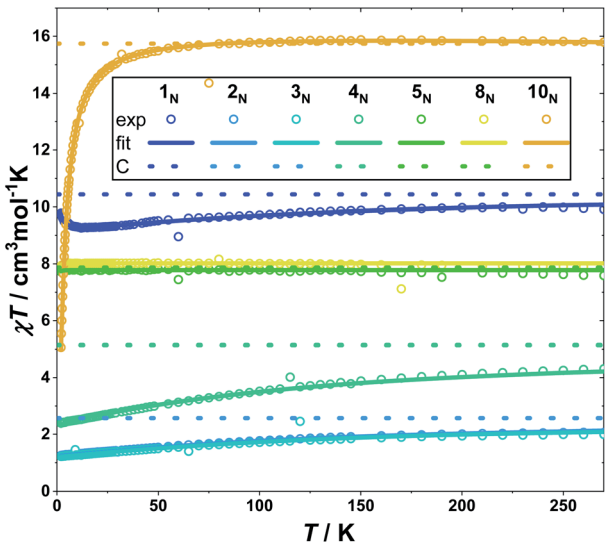

Fig. 5 χT products of $\mathbf{1_N}$–$\mathbf{5_N}$, $\mathbf{8_N}$ and $\mathbf{10_N}$ (scatter) with best fits (lines) as described in the text.

The quantitative analysis of the static magnetic properties of the studied complexes was performed by simultaneous numerical fitting, by use of the simplex algorithm,[86] of both the χT and VTVB data to Hamiltonian (**1**)

$$\hat{H} = \sum_{i=1,2} \left\{ \mu_B \vec{B} g_J \hat{J} + \sum_{\substack{k=2,4,6 \\ -k \le q \le k}} B_k^q \hat{O}_k^q \right\}_i + \hat{J}_1 \tilde{J}_{12} \hat{J}_2 \qquad (1)$$

where the first term is the Zeeman interaction, with μ_B the Bohr magneton, $\vec{B}$ the magnetic field vector, and g_J and $\hat{J}$ the Landé g-factor and total spin–orbit angular momentum operator of multiplet J, respectively. The second term expresses the crystal field (CF), with B_k^q the parameter associated to operator $\hat{O}_k^q$, within the Steven's formalism. The third term accounts for the magnetic exchange between Ln centres, with $\tilde{J}_{12}$ being a general second order exchange tensor that can be decomposed into isotropic, J_{12}, antisymmetric, d_{12}, and anisotropic, D_{12}, contributions.[87] Not all terms in the general expression of (**1**) are relevant for the analysis of the magnetic properties of all the studied complexes. The summation over Zeeman and CF terms, as well as the exchange term, are relevant only for complexes containing two paramagnetic centres. For orbitally non-degenerate ions, such as Gd(III), inclusion of only isotropic exchange terms in the Hamiltonian is sufficient. For orbitally degenerate ions, such as Yb(III), anisotropic exchange terms must be considered.[88] Here, for the sake of simplicity, we consider exchange anisotropy terms only up to second order (D_{12}) and neglect antisymmetric interactions.

We performed the quantitative analysis of the static magnetic properties in two steps. Initially the CF parameters of Gd(III) or Yb(III) sites in complexes containing only a paramagnetic centre ($\mathbf{2_N}$, $\mathbf{3_N}$, $\mathbf{5_N}$ and $\mathbf{8_N}$) were determined. The number of CF parameters required depends on the symmetry of the coordination sphere of the Ln ion. For C_1 symmetry, as is

Open Access Article. Published on 15 April 2021. Downloaded on 11/22/2025 9:41:00 PM. This article is licensed under a Creative Commons Attribution-NonCommercial 3.0 Unported Licence.

the case for $\mathbf{2_N}$, $\mathbf{3_N}$, $\mathbf{5_N}$ and $\mathbf{8_N}$, twenty seven CF parameters are needed. Determining this number of parameters from the magnetic susceptibility and VTVB measurements alone would result in overparameterization. To remediate this problem, we assume that the local symmetry of the Ln sites is C_3, neglecting the effect of the coordinated nitrate anions. By assuming C_3 symmetry, the maximum number of CF parameters reduces to nine. However, nine CF parameters is still a large number of parameters to be determined solely from thermodynamic magnetization data. Thus, additional information can be incorporated in the fitting model by exploiting emission and Electron Paramagnetic Resonance (EPR) spectroscopies, as has been previously shown for the Ln(trensal) series.[45–54] Once the CF parameters of Gd(III) and Yb(III) sites determined, quantitative analysis of the magnetic properties of complexes containing two paramagnetic centres was performed by fixing the CF parameters of Gd(III) and/or Yb(III) and fitting only the parameters relevant to the exchange term of Hamiltonian (**1**).

In the case of complexes containing a paramagnetic Gd(III) ion and a diamagnetic Lu(III) or Y(III) ion ($\mathbf{5_N}$ and $\mathbf{8_N}$, respectively), the $4f^7$ electronic configuration of Gd(III) results in an $^8S_{7/2}$ ground term where the orbital angular momentum is quenched. This means that there are no first order contributions to anisotropy and that the associated CF splitting is relatively small with respect to the experimental conditions of magnetization measurements. Hence, very little information on the CF can be extracted solely from magnetization measurements. However, the small CF in Gd(III) means that all transitions within the ground multiplet can be observed using EPR spectroscopy and thus information on the CF parameters can be extracted based on these observations. Using the EPR simulation software Sim,[89] the EPR spectra of $\mathbf{5_N}$ and $\mathbf{8_N}$ were simulated using Hamiltonian (**1**) resulting in the best-fit CF parameters (in Stevens formalism[90]): $B_2^0/hc = -1.84 \times 10^{-2}$ cm^{-1}, $B_4^0/hc = 1.95 \times 10^{-4}$ cm^{-1} and $B_6^0/hc = -6.67 \times 10^{-6}$ cm^{-1} with $g = 2$ and h and c the Planck and speed of light constants (Fig. S84 and S85†). Because of the very broad polycrystalline powder EPR spectra no off-diagonal CF parameters could be determined. The obtained CF parameters were then used to simulate the χT product and the VTVB data (Fig. 5, S78 and S79†). The associated eigen-spectrum is shown in Fig. S91† where it can be seen that the total CF splitting of $\mathbf{5_N}$ and $\mathbf{8_N}$ is of the order of 1 cm^{-1}. We note that both complexes display very similar EPR spectra, albeit very broad (Fig. S84 and S85†), suggesting that the CF of Gd(III) is not dramatically influenced by the size of the second Ln ion.

For the complexes containing a paramagnetic Yb(III) ion and a diamagnetic Y(III) or Lu(III) ion ($\mathbf{2_N}$ and $\mathbf{3_N}$, respectively), the $4f^{13}$ electronic configuration of Yb(III) results in an $^2F_{7/2}$ ground term where the orbital angular momentum of Yb(III) is unquenched. Thus, anisotropy to first order is expected for the CF splitting pattern of Yb(III). This means that in the case of Yb(III), emission spectroscopy can be exploited, in addition to EPR, as an additional source of information on the CF. The solid state, room temperature emission spectra of $\mathbf{2_N}$ and $\mathbf{3_N}$, diluted at 3% in the diamagnetic host $\mathbf{9_N}$, reveal that the total CF splitting of the ground term of Yb(III) in these complexes is of the order of 560 cm^{-1} (Fig. S88†). This is approximately 2/3 of the value observed in the parent Ln(trensal) complex,[46] evidencing the influence of the electron density of one Ln centre as an additional contribution to the ligand field of the other one. However, the polycrystalline powder EPR spectra of these dilute samples of $\mathbf{2_N}$ and $\mathbf{3_N}$, are too broad (Fig. S86 and S87†) to offer reliable information to be used in the fitting procedure. Furthermore, the χT products and VTVB measurements of $\mathbf{2_N}$ and $\mathbf{3_N}$ are very similar (Fig. 5, S70 and S72†). This suggests that the CF of Yb(III) in these two complexes is very similar, and similar to that observed for Gd(III) in $\mathbf{5_N}$ and $\mathbf{8_N}$. Therefore, CF parameters were extracted only from measurements on $\mathbf{2_N}$. Thus, the CF parameters of $\mathbf{2_N}$ were obtained by simultaneously fitting to Hamiltonian (**1**) its χT product, VTVB data and total multiplet splitting, determined by emission spectroscopy. As initial parameters for the modelling, the CF parameters of YbL were used.[83] Using this model and allowing all nine CF parameters to vary, good agreement between the predicted and measured VTVB and susceptibility curves was obtained (Fig. 5 and S70†). The nine best-fit CF parameters are given in Tables S1 and S2† in Stevens and Wybourne notations, respectively. The associated eigenspectrum is shown in Fig. S91† where it can be seen that the total CF splitting of $\mathbf{2_N}$ and $\mathbf{3_N}$ is of the order of 560 cm^{-1}. This set of parameters also reproduces the susceptibility and VTVB measurements of $\mathbf{3_N}$, demonstrating that the CF of Yb(III) in these complexes does not dramatically depend on the size of the second Ln ion (Fig. S71 and S72†).

For the complexes containing two paramagnetic Ln ions ($\mathbf{10_N}$, $\mathbf{1_N}$ and $\mathbf{4_N}$) inclusion of exchange interaction terms in Hamiltonian (**1**) is necessary since statistically significant deviations are observed between the experimental χT product of these as compared to the sum of their uncorrelated constitutive centres (Fig. S81–S83†).

In the case of $\mathbf{10_N}$, the magnetic exchange interaction between the two Gd(III) centers can be treated by including in Hamiltonian (**1**) only isotropic exchange terms ($J_{\mathrm{Gd-Gd}}$). Thus, by fixing the CF parameters of Gd(III) to the ones determined for $\mathbf{5_N}$ and $\mathbf{8_N}$, $J_{\mathrm{Gd-Gd}}/hc$ was determined to be -0.1370 cm^{-1} $\pm$ 0.0005 cm^{-1} (in the $-2J$ convention), by a simultaneous fit of the χT product and the VTVB data to Hamiltonian (**1**). The model reproduced the measurements well, with an antiferromagnetic interaction between the two Gd(III) ions (Fig. 5 and S80†). The associated eigenspectrum of $\mathbf{10_N}$ is shown in Fig. S91† where it can be seen that the antiferromagnetic interactions in $\mathbf{10_N}$ result in a group of sixty four closely packed states, spread over a total range of $\sim$9 cm^{-1}. The antiferromagnetic ground state is a singlet separated from the first excited state by just 0.05 cm^{-1}. The determined best-fit value is lower than that previously reported ($J_{\mathrm{iso}}/hc = -0.194$ cm^{-1}) for this complex using a spin-only expression,[80] where only magnetic susceptibility data (not VTVB data) were analyzed.

For $\mathbf{1_N}$ and $\mathbf{4_N}$ containing the orbitally degenerate Yb(III) ion, anisotropic exchange, in addition to isotropic exchange, should be included. However, such a model (Table S3†) produces the same results, on a qualitative level, irrespective of whether the model contains only isotropic exchange (Fig. 5), only anisotropic exchange, or both anisotropic and isotropic exchange

 © 2021 The Author(s). Published by the Royal Society of Chemistry

Open Access Article. Published on 15 April 2021. Downloaded on 11/22/2025 9:41:00 PM. This article is licensed under a Creative Commons Attribution-NonCommercial 3.0 Unported Licence.

(Fig. S65–S68 and S73–S76†). This is most likely due to the fact that the polycrystalline powder data used in the modelling are insufficient to probe the orientation sensitivity of the anisotropic exchange terms, as previously discussed.[88] Small crystal size precludes orientation dependent single crystal magnetization and EPR measurements. Performing the modelling without including exchange terms results in poorer agreement with experiment, clearly demonstrating that magnetic exchange interactions are operating in $\mathbf{1_N}$ and $\mathbf{4_N}$ (Fig. S65–S69† for $\mathbf{1_N}$ and Fig. S73–S77† for $\mathbf{4_N}$). This is also observed in the temperature dependence of the χT product of $\mathbf{1_N}$, which increases upon cooling from 12 to 2 K. Using only an isotropic exchange term in $\mathbf{1_N}$ and $\mathbf{4_N}$ yielded a ferromagnetic interaction in $\mathbf{1_N}$ ($J_{iso}/hc = 0.01780\ cm^{-1} \pm 0.00005\ cm^{-1}$) and an anti-ferromagnetic interaction in $\mathbf{4_N}$ ($J_{iso}/hc = -0.0072\ cm^{-1} \pm 0.0007\ cm^{-1}$). The associated eigenspectra of $\mathbf{1_N}$ and $\mathbf{4_N}$ are shown in Fig. S91.† In the case of $\mathbf{1_N}$ the sixty four levels are grouped into four sets of sixteen, corresponding to the interaction of each of the four Kramers doublets of Yb(III) with the four Kramers doublets of Gd(III), spread over a range of ~700 cm^{-1}. In the case of $\mathbf{4_N}$ the sixty four levels are grouped in ten sets spread over a range of ~1100 cm^{-1}.

Conclusions

We have developed a synthetic strategy for the synthesis of pure heterodinuclear Ln cryptate complexes, of arbitrary composition. The LnLn* distribution obtained through this synthetic protocol is dependent on the counterion used. The presence of nitrate instead of triflate leads to scrambling of the Ln ions. This suggests that the Lewis basicity of the counter ion is crucial. The Brønsted basicity of the solvent also proved crucial in controlling the scrambling ratio, with pyridine offering the best control. Complexes $\mathbf{1_N}$–$\mathbf{10_N}$ are all obtained in the same crystal phase, with the complexes crystallizing in one of the enantiomorphic space groups $P4_12_12$ or $P4_32_12$. These chiral Ln complexes that display sizeable spin–orbit coupling interactions will be of particular interest for probing electric field effects on their magnetization *via* magnetoelectric coupling,[91,92] which is relevant to the development of molecular spintronic devices.

The Ln–Ln distance, bridged by three phenoxide O-atoms, was found to be ~3.5 Å with GdGd having the largest distance at 3.5035(7) Å and LuLu possessing the smallest distance at 3.4396(7) Å. This results in relatively strong magnetic exchange coupling between the metals with respect to QIP protocols. For both $\mathbf{4_N}$ and $\mathbf{10_N}$ the lanthanide ions are coupled antiferromagnetically. On the contrary, $\mathbf{1_N}$ shows ferromagnetic coupling between the two lanthanide ions. In future studies on single crystals, the exchange coupling between the isotropic Gd(III) ion and oblate or prolate Ln(III) ions, as well the coupling between two anisotropic ions, will be investigated in detail.

Author contributions

Christian D. Buch was involved as major contributor to all of the described experimental work and the theoretical modelling of the data and drafted early versions of the manuscript. Steen H. Hansen, Dmitri Mitcov and Camilla M. Tram were involved in the development of the synthetic protocol. Gary S. Nichol and Euan K. Brechin were involved in the crystallographic studies. Stergios Piligkos conceived and supervised the project and wrote the manuscript with contributions and comments from all authors.

Conflicts of interest

There are no conflicts to declare.

Acknowledgements

SP thanks the VILLUM FONDEN for research grant 13376.

Notes and references

1 S. R. Tamang, A. Singh, D. Bedi, A. R. Bazkiaei, A. A. Warner, K. Glogau, C. McDonald, D. K. Unruh and M. Findlater, *Nat. Catal.*, 2020, **3**, 154–162.
2 Y. Qiao and E. J. Schelter, *Acc. Chem. Res.*, 2018, **51**, 2926–2936.
3 G. N. Trinadhachari, A. G. Kamat, K. J. Prabahar, V. K. Handa, K. N. V. S. Srinu, K. R. Babu and P. D. Sanasi, *Org. Process Res. Dev.*, 2013, **17**, 406–412.
4 S. Kobayashi, T. Hamada, S. Nagayama and K. Manabe, *Org. Lett.*, 2001, **3**, 165–167.
5 H. C. Aspinall, J. L. M. Dwyer, N. Greeves and A. Steiner, *Organometallics*, 1999, **18**, 1366–1368.
6 D. Goldfarb, *Phys. Chem. Chem. Phys.*, 2014, **16**, 9685–9699.
7 J. A. Cotruvo Jr, *ACS Cent. Sci.*, 2019, **5**, 1496–1506.
8 P. Caravan, J. J. Ellison, T. J. McMurry and R. B. Lauffer, *Chem. Rev.*, 1999, **99**, 2293–2352.
9 A. D. Sherry, P. Caravan and R. E. Lenkinski, *J. Magn. Reson. Imaging*, 2009, **30**, 1240–1248.
10 J. Wahsner, E. M. Gale, A. Rodriguez-Rodriguez and P. Caravan, *Chem. Rev.*, 2019, **119**, 957–1057.
11 J.-C. G. Bünzli, *Chem. Rev.*, 2010, **110**, 2729–2755.
12 T. Gunnlaugsson and J. P. Leonard, *Chem. Commun.*, 2005, 3114–3131, DOI: 10.1039/b418196d.
13 K. Lee, V. Dzubeck, L. Latshaw and J. P. Schneider, *J. Am. Chem. Soc.*, 2004, **126**, 13616–13617.
14 C. Wei, L. Ma, H. Wei, Z. Liu, Z. Bian and C. Huang, *Sci. China: Technol. Sci.*, 2018, **61**, 1265–1285.
15 R. Yan, Y. Hu, F. Liu, S. Wei, D. Fang, A. J. Shuhendler, H. Liu, H.-Y. Chen and D. Ye, *J. Am. Chem. Soc.*, 2019, **141**, 10331–10341.
16 V. S. R. Harrison, C. E. Carney, K. W. MacRenaris, E. A. Waters and T. J. Meade, *J. Am. Chem. Soc.*, 2015, **137**, 9108–9116.
17 M. Benezra, O. Penate-Medina, P. B. Zanzonico, D. Schaer, H. Ow, A. Burns, E. DeStanchina, V. Longo, E. Herz, S. Iyer, J. Wolchok, S. M. Larson, U. Wiesner and M. S. Bradbury, *J. Clin. Invest.*, 2011, **121**, 2768–2780.
18 R. Sessoli and A. K. Powell, *Coord. Chem. Rev.*, 2009, **253**, 2328–2341.

Open Access Article. Published on 15 April 2021. Downloaded on 11/22/2025 9:41:00 PM.
This article is licensed under a Creative Commons Attribution-NonCommercial 3.0 Unported Licence.

19 S. T. Liddle and J. van Slageren, *Chem. Soc. Rev.*, 2015, **44**, 6655–6669.
20 S. Demir, M. I. Gonzalez, L. E. Darago, W. J. Evans and J. R. Long, *Nat. Commun.*, 2017, **8**, 2144.
21 J. D. Rinehart, M. Fang, W. J. Evans and J. R. Long, *Nat. Chem.*, 2011, **3**, 538–542.
22 K. S. Pedersen, A. M. Ariciu, S. McAdams, H. Weihe, J. Bendix, F. Tuna and S. Piligkos, *J. Am. Chem. Soc.*, 2016, **138**, 5801–5804.
23 M. D. Jenkins, Y. Duan, B. Diosdado, J. J. García-Ripoll, A. Gaita-Ariño, C. Giménez-Saiz, P. J. Alonso, E. Coronado and F. Luis, *Phys. Rev. B*, 2017, **95**, 064423.
24 M. Shiddiq, D. Komijani, Y. Duan, A. Gaita-Arino, E. Coronado and S. Hill, *Nature*, 2016, **531**, 348–351.
25 R. Hussain, G. Allodi, A. Chiesa, E. Garlatti, D. Mitcov, A. Konstantatos, K. S. Pedersen, R. De Renzi, S. Piligkos and S. Carretta, *J. Am. Chem. Soc.*, 2018, **140**, 9814–9818.
26 G. Handzlik, M. Magott, M. Arczynski, A. M. Sheveleva, F. Tuna, M. Sarewicz, A. Osyczka, M. Rams, V. Vieru, L. F. Chibotaru and D. Pinkowicz, *J. Phys. Chem. Lett.*, 2020, **11**, 1508–1515.
27 P. Siyushev, K. Xia, R. Reuter, M. Jamali, R. Kolesov, J. Wrachtrup, N. Zhao, N. Yang, C. Duan, N. Kukharchyk and A. D. Wieck, *Nat. Commun.*, 2014, **5**, 3895.
28 S. Thiele, F. Balestro, R. Ballou, S. Klyatskaya, M. Ruben and W. Wernsdorfer, *Science*, 2014, **344**, 1135–1138.
29 R. Vincent, S. Klyatskaya, M. Ruben, W. Wernsdorfer and F. Balestro, *Nature*, 2012, **488**, 357–360.
30 Y.-S. Ding, Y.-F. Deng and Y.-Z. Zheng, *Magnetochemistry*, 2016, **2**, 40.
31 D. Aguila, L. A. Barrios, V. Velasco, O. Roubeau, A. Repolles, P. J. Alonso, J. Sese, S. J. Teat, F. Luis and G. Aromi, *J. Am. Chem. Soc.*, 2014, **136**, 14215–14222.
32 G. Aromi, D. Aguila, P. Gamez, F. Luis and O. Roubeau, *Chem. Soc. Rev.*, 2012, **41**, 537–546.
33 V. Velasco, L. A. Barrios, M. Schutze, O. Roubeau, F. Luis, S. J. Teat, D. Aguila and G. Aromi, *Chemistry*, 2019, **25**, 15228–15232.
34 E. Macaluso, M. Rubín, D. Aguilà, A. Chiesa, L. A. Barrios, J. I. Martínez, P. J. Alonso, O. Roubeau, F. Luis, G. Aromí and S. Carretta, *Chem. Sci.*, 2020, **11**, 10337–10343.
35 C. E. Housecroft and A. G. Sharpe, *Inorganic Chemistry*, Pearson Education Limited, 3rd edn, 2008.
36 D. Gatteschi, R. Sessoli and J. Villain, *Molecular Nanomagnets*, Oxford University Press, New York, 2007.
37 R. Winpenny, *Single-Molecule Magnets and Related Phenomena*, Springer-Verlag Berlin Heidelberg, Berlin, Heidelberg, 2006.
38 D. N. Woodruff, R. E. Winpenny and R. A. Layfield, *Chem. Rev.*, 2013, **113**, 5110–5148.
39 F. S. Guo, B. M. Day, Y. C. Chen, M. L. Tong, A. Mansikkamaki and R. A. Layfield, *Science*, 2018, **362**, 1400–1403.
40 C. A. P. Goodwin, F. Ortu, D. Reta, N. F. Chilton and D. P. Mills, *Nature*, 2017, **548**, 439–442.
41 K. Randall McClain, C. A. Gould, K. Chakarawet, S. J. Teat, T. J. Groshens, J. R. Long and B. G. Harvey, *Chem. Sci.*, 2018, **9**, 8492–8503.
42 D. Aguila, L. A. Barrios, V. Velasco, O. Roubeau, A. Repolles, P. J. Alonso, J. Sese, S. J. Teat, F. Luis and G. Aromi, *J. Am. Chem. Soc.*, 2014, **136**, 14215–14222.
43 F. Luis, A. Repolles, M. J. Martinez-Perez, D. Aguila, O. Roubeau, D. Zueco, P. J. Alonso, M. Evangelisti, A. Camon, J. Sese, L. A. Barrios and G. Aromi, *Phys. Rev. Lett.*, 2011, **107**, 117203.
44 M. Shiddiq, D. Komijani, Y. Duan, A. Gaita-Arino, E. Coronado and S. Hill, *Nature*, 2016, **531**, 348–351.
45 K. S. Pedersen, A.-M. Ariciu, S. McAdams, H. Weihe, J. Bendix, F. Tuna and S. Piligkos, *J. Am. Chem. Soc.*, 2016, **138**, 5801–5804.
46 K. S. Pedersen, J. Dreiser, H. Weihe, R. Sibille, H. V. Johannesen, M. A. Soerensen, B. E. Nielsen, M. Sigrist, H. Mutka, S. Rols, J. Bendix and S. Piligkos, *Inorg. Chem.*, 2015, **54**, 7600–7606.
47 P. V. Bernhardt, B. M. Flanagan and M. J. Riley, *Aust. J. Chem.*, 2000, **53**, 229–231.
48 P. V. Bernhardt, B. M. Flanagan and M. J. Riley, *Aust. J. Chem.*, 2001, **54**, 229–232.
49 P. V. Bernhardt, B. M. Flanagan, M. J. Riley and B. J. Wood, *J. Electron Spectrosc. Relat. Phenom.*, 2002, **124**, 73–77.
50 B. M. Flanagan, P. V. Bernhardt, E. R. Krausz, S. R. Luthi and M. J. Riley, *Inorg. Chem.*, 2001, **40**, 5401–5407.
51 B. M. Flanagan, P. V. Bernhardt, E. R. Krausz, S. R. Luthi and M. J. Riley, *Inorg. Chem.*, 2002, **41**, 5024–5033.
52 E. Lucaccini, L. Sorace, M. Perfetti, J. P. Costes and R. Sessoli, *Chem. Commun.*, 2014, **50**, 1648–1651.
53 E. Lucaccini, L. Sorace, F. Adelnia, S. Sanna, P. Arosio, M. Mariani, S. Carretta, Z. Salman, F. Borsa and A. Lascialfari, *Phys. Rev. B*, 2019, **100**, 174416.
54 J. Dreiser, G. E. Pacchioni, F. Donati, L. Gragnaniello, A. Cavallin, K. S. Pedersen, J. Bendix, B. Delley, M. Pivetta, S. Rusponi and H. Brune, *ACS Nano*, 2016, **10**, 2887–2892.
55 S. S. Bullock, D. P. O'Leary and G. K. Brennen, *Phys. Rev. Lett.*, 2005, **94**, 230502.
56 A. C. Dada, J. Leach, G. S. Buller, M. J. Padgett and E. Andersson, *Nat. Phys.*, 2011, **7**, 677–680.
57 M. D. Jenkins, Y. Duan, B. Diosdado, J. J. Garcia-Ripoll, A. Gaita-Arino, C. Gimenez-Saiz, P. J. Alonso, E. Coronado and F. Luis, *Phys. Rev. B*, 2017, **95**, 064423.
58 E. O. Kiktenko, A. K. Fedorov, A. A. Strakhov and V. I. Man'ko, *Phys. Lett. A*, 2015, **379**, 1409–1413.
59 M. Neeley, M. Ansmann, R. C. Bialczak, M. Hofheinz, E. Lucero, A. D. O'Connell, D. Sank, H. Wang, J. Wenner, A. N. Cleland, M. R. Geller and J. M. Martinis, *Science*, 2009, **325**, 722–725.
60 C. Godfrin, A. Ferhat, R. Ballou, W. Wernsdorfer, F. Balestro, C. Godfrin, A. Ferhat, R. Ballou, W. Wernsdorfer, F. Balestro, S. Klyatskaya, M. Ruben, W. Wernsdorfer and F. Balestro, *Phys. Rev. Lett.*, 2017, **119**, 187702.
61 J. A. Jones, *Prog. Nucl. Magn. Reson. Spectrosc.*, 2011, **59**, 91–120.

 © 2021 The Author(s). Published by the Royal Society of Chemistry

Open Access Article. Published on 15 April 2021. Downloaded on 11/22/2025 9:41:00 PM.
This article is licensed under a Creative Commons Attribution-NonCommercial 3.0 Unported Licence.

62 Y. Zhang, C. A. Ryan, R. Laflamme and J. Baugh, *Phys. Rev. Lett.*, 2011, **107**, 170503.
63 R. Hussain, G. Allodi, A. Chiesa, E. Garlatti, D. Mitcov, A. Konstantatos, K. S. Pedersen, R. De Renzi, S. Piligkos and S. Carretta, *J. Am. Chem. Soc.*, 2018, **140**, 9814–9818.
64 E. Moreno-Pineda, C. Godfrin, F. Balestro, W. Wernsdorfer and M. Ruben, *Chem. Soc. Rev.*, 2018, **47**, 501–513.
65 M. Atzori, A. Chiesa, E. Morra, M. Chiesa, L. Sorace, S. Carretta and R. Sessoli, *Chem. Sci.*, 2018, **9**, 6183–6192.
66 J.-P. Costes, F. Nicodème, T. Ayabe, M. Takeda and M. Takahashi, *Polyhedron*, 2019, **174**, 114154.
67 D. Aguila, V. Velasco, L. A. Barrios, J. Gonzalez-Fabra, C. Bo, S. J. Teat, O. Roubeau and G. Aromi, *Inorg. Chem.*, 2018, **57**, 8429–8439.
68 J. D. Leng, J. L. Liu, Y. Z. Zheng, L. Ungur, L. F. Chibotaru, F. S. Guo and M. L. Tong, *Chem. Commun.*, 2013, **49**, 158–160.
69 F. Tanaka and T. Ishibashi, *J. Chem. Soc., Faraday Trans.*, 1996, **92**, 1105–1110.
70 J. J. Le Roy, J. Cremers, I. A. Thomlinson, M. Slota, W. K. Myers, P. H. Horton, S. J. Coles, H. L. Anderson and L. Bogani, *Chem. Sci.*, 2018, **9**, 8474–8481.
71 N. Ishikawa, T. Iino and Y. Kaizu, *J. Am. Chem. Soc.*, 2002, **124**, 11440–11447.
72 N. Ishikawa, T. Iino and Y. Kaizu, *J. Phys. Chem. A*, 2002, **106**, 9543–9550.
73 D. Chabach, A. De Cian, J. Fischer, R. Weiss and M. E. M. Bibout, *Angew. Chem., Int. Ed. Engl.*, 1996, **35**, 898–899.
74 S. Faulkner and S. J. Pope, *J. Am. Chem. Soc.*, 2003, **125**, 10526–10527.
75 L. S. Natrajan, A. J. Villaraza, A. M. Kenwright and S. Faulkner, *Chem. Commun.*, 2009, 6020–6022, DOI: 10.1039/b913702e.
76 T. J. Sorensen, M. Tropiano, O. A. Blackburn, J. A. Tilney, A. M. Kenwright and S. Faulkner, *Chem. Commun.*, 2013, **49**, 783–785.
77 J. M. Lehn and J. P. Sauvage, *J. Am. Chem. Soc.*, 1975, **97**, 6700–6707.
78 C. Platas, F. Avecilla, A. de Blas, T. Rodríguez-Blas, C. F. G. C. Geraldes, É. Tóth, A. E. Merbach and J.-C. G. Bünzli, *J. Chem. Soc., Dalton Trans.*, 2000, 611–618, DOI: 10.1039/a906675f.
79 F. Avecilla, A. de Blas, C. Platas, T. Rodríguez-Blas, R. Bastida, A. Macías, A. Rodríguez, D. E. Fenton and J. Mahía, *Chem. Commun.*, 1999, 125–126, DOI: 10.1039/a807435f.
80 F. Avecilla, C. Platas-Iglesias, R. Rodríguez-Cortiñas, G. Guillemot, J.-C. G. Bünzli, C. D. Brondino, C. F. G. C. Geraldes, A. d. Blas and T. Rodríguez-Blas, *J. Chem. Soc., Dalton Trans.*, 2002, 4658–4665.
81 F. Avecilla, R. Bastida, A. d. Blas, E. Carrera, D. E. Fenton, A. Macías, C. Platas, A. Rodríguez and T. Rodríguez-Blas, *Z. Naturforsch., B: J. Chem. Sci.*, 1997, **52**, 1273–1277.
82 M. Kanesato, H. Houjou, Y. Nagawa and K. Hiratani, *Inorg. Chem. Commun.*, 2002, **5**, 984–988.
83 C. D. Buch, D. Mitcov and S. Piligkos, *Dalton Trans.*, 2020, **49**, 13557–13565.
84 C. D. Buch, S. H. Hansen, C. M. Tram, D. Mitcov and S. Piligkos, *Inorg. Chem.*, 2020, **59**, 16328–16340.
85 H. D. Flack, *Helv. Chim. Acta*, 2003, **86**, 905–921.
86 W. H. Press, B. P. Flannery, S. A. Teukolsky and W. T. Vetterling, *Numerical recipes: the art of scientific computing*, Cambridge University Press, Cambridge, 1992.
87 D. Gatteschi, R. Sessoli and J. Villain, *Molecular Nanomagnets*, Oxford University Press, New York, 2007.
88 L. Sorace and D. Gatteschi, in *Lanthanides and Actinides in Molecular Magnetism*, 2015, pp. 1–26, DOI: 10.1002/9783527673476.ch1.
89 Q. Scheifele, T. Birk, J. Bendix, P. L. W. Tregenna-Piggott and H. Weihe, *Angew. Chem., Int. Ed.*, 2008, **47**, 148–150.
90 A. Abragam and B. Bleaney, *Electron Paramagnetic Resonance of Transition Ions*, Dover, 1986.
91 M. Trif, F. Troiani, D. Stepanenko and D. Loss, *Phys. Rev. Lett.*, 2008, **101**, 217201.
92 M. Fittipaldi, A. Cini, G. Annino, A. Vindigni, A. Caneschi and R. Sessoli, *Nat. Mater.*, 2019, **18**, 329–334.